Available online at www.ilcpa.pl

International Letters of Chemistry, Physics and Astronomy

17(2) (2014) 125-141 ISSN 2299-3843

Studies on spray pyrolised nanostructured SnO_2 thin films for H_2 gas sensing application

R. H. Bari*, S. B. Patil

Nanomaterials Research Laboratory, Department of Physics,
G. D. M. Arts, K. R. N. Commerce and M.D. Science College, Jamner 424 206, India
*Tel.: +91 9423914198

*E-mail address: rameshbari24@yahoo.com

ABSTRACT

The objective of this work is to study the influence of pyrolysis temperature on structural, surface morphology and gas sensing properties of the nanostructured SnO_2 thin films prepared by spray pyrolysis technique. These films were characterized for the structural, morphological and elemental composition carried by means of X-ray diffraction (XRD), scanning electron microscopy (SEM) and energy dispersive spectrophotometer (EDAX). The information of crystallite size, dislocation density and microstrain is obtained from the full width-at half- maximum (FWHM) of the diffraction peaks. Effect of sprayed deposition temperature on H_2 gas sensing performance and electrical properties were studied using static gas sensing system. The sensor ($T_{pyr.}$ = 350 °C) showed high gas response (S = 1200 at 350 °C) on exposure of 500 ppm of H_2 and high selectivity against other gases The results are discussed and interpreted.

***Keywords*:** Spray Pyrolysis; Nanostructured SnO_2; Thin films; H_2 gas sensor; Microstrain; Electrical conductivity

1. INTRODUCTION

Tin oxide (SnO_2) is wide band gap an *n*-type semiconductor of tetragonal structure, which can be efficiently used as transparent conducting oxide. Because of its unique electrical and optical properties [1-2]. It has some advantage over other possible materials such as CdO, In_2O_3, ZnO or Cd_2SnO_4 due to its unique combination of interesting properties: non-toxicity, good electrical, optical and piezoelectric behavior and its low price. There is an increasing demand for SnO_2 semiconductor metal oxide (SMO) for several application that have silicon solar cells, liquid crystal display, gas sensor and many more [3-5], mainly due to their outstanding properties.

Nanostructured tin oxide (SnO_2) thin films have been prepared by various deposition techniques such as ultrasonic spray pyrolysis, chemical vapour deposition, activated reactive evaporation, ion-beam assisted deposition, sputtering and sol-gel [6-11] methods.

The methods that have are used more often for depositing nanostructured tin oxide thin films were ultrasonic spray pyrolysis, chemical vapour deposition, activated reactive evaporation, ion-beam assisted deposition, sputtering and sol-gel [6-11] methods. Of these methods, the spray pyrolysis is unique and cost effective compared to other methods requiring high vacuum environment. It is one step method operating at atmospheric pressure with very short production time [12]. Spray pyrolysis has proved to be simple, reproducible and inexpensive, as well as suitable for large area applications. Besides the simple experimental arrangement, high growth rate and mass production capability for large area coatings make them useful for industrial as well as solar cell applications. By using this technique one can control the film morphology and particle size in the nanometer range.

In the present investigations, nanostructured SnO_2 thin films with different spray pyrolysis temperature were prepared using spray pyrolysis technique. Structural and microstructural properties were studied using X-ray diffractogram and SEM. Study of elemental composition was carried out using EDAX. Electrical conductivity and gas sensing properties were studied using static gas sensing system at different operating temperature.

2. EXPERIMENTAL DETAILS

2. 1. Substrate Cleaning

All the chemical reagents used in the experiments were obtained from commercial sources as guaranteed-grade reagents and used without further purification. The glass substrates supplied by Blue Star Mumbai, were used to deposit the SnO_2 thin films. Before the deposition of SnO_2 thin films, glass slides were cleaned with detergent and distilled water, then boiled in chromic acid (0.5 M) for 25 min, then slides washed with double distilled water and further ultrasonically cleaned for 15 min. Finally the substrates were degreased in AR grade acetone and used for spray deposition technique [13].

2. 2. Nanostructured Thin films preparation set-up

Nanostructured SnO_2 films were prepared on preheated glass substrate using a spray pyrolysis technique and the experimental set up is described elsewhere [13]. Spray pyrolysis is basically a chemical process, which consists of a solution that is sprayed onto a hot substrate held at high temperature, where the solution reacts to form the desired thin film.

The spraying solution was prepared by mixing the appropriate volumes of 0.05 M tin (II) tin chloride (IV) pentahydrate ($SnCl_4 \cdot 5H_2O$), (Purified Sigma Aldrich) in de-ionized water as a precursor. The SnO_2 films were deposited at different substrate temperatures of 300, 350 and 400 °C. Samples deposited at various substrate temperatures are denoted by S1, S2 and S3, where numbers stand for substrate temperatures. The optimized values of important preparative parameters are shown in Table 1. Spray rate (7 ml/min), distance between substrate to nozzle (30 cm), solution concentration (0.05 M) and quantity of the spraying solution (30 ml).

After the deposition, the films were allowed to cool naturally at room temperature. All the films were adherent to the substrate, were further used for structural, and morphological characterizations. The pyrolytic reaction takes place on a heated substrate, leading to a nanostructured SnO_2. The usual expression for this reaction is:

$$SnCl_4 \cdot 5H_2O \rightarrow SnO_2 + 3H_2O \uparrow + 4HCl \uparrow \qquad \text{------- (1)}$$

2. 3. Optimized parameters

Table 1 shows the optimized parameters for the preparation of nanostructured SnO_2 thin films.

Table 1. Optimum parameter to obtain nanostructured SnO_2 thin films.

Spray parameter	Optimum value / item
Nozzle	Glass
Nozzle to substrate distance	30 cm
$SnCl_4 \cdot 5H_2O$ solution concentration	0.05 M
Solvent	De-ionised water
Solution flow rate	7 ml / min.
Carrier gas	Compressed air
Substrate deposition temperature (Tpyr.)	300 °C, 350 °C, and 400 °C

2. 4. Annealing of SnO_2 thin films

The as prepared nanostructured SnO_2 thin film samples S1, S2, and S3 were annealed at 500 °C for 1 h.

2. 5. Sensing system to test the gases

The gas sensing studies were carried out using a static gas chamber to sense H_2 gas in air ambient. The nanocrystalline SnO_2 thin films were used as the sensing elements. Cr-Al thermocouple is mounted to measure the temperature. The output of thermocouple is connected to temperature indicator. Gas inlet valve fitted at one of the ports of the base plate. Gas concentration (500 ppm) inside the static system is achieved by injecting a known volume of test gas in gas injecting syringe. Constant voltage (5V) is applied to the sensor and current can be measured by picoammeter.

2. 6. Thin film characterizations

The Nanostructured SnO_2 thin film were characterized by X-ray diffraction ((Miniflex Model, Rigaku, Japan)) using CuKα radiation with a wavelength, λ = 1·5418 Å. The microstructure and elemental composition of the films was analyzed using scanning electron microscope coupled with energy dispersive spectrophotometer (SEM, JEOL. JED 6300). Electrical conductivity and gas sensing studies were conducted using home built gas sensing set up.

3. RESULTS AND DISCUSSION

3. 1. Determination of film thickness

Film thickness was measured by using a micro gravimetrical method [14] (considering the density of the bulk tin oxide). The films were deposited on clean glass slides whose mass

was previously determined. After the deposition the substrate was again weighted, determining the quantity of deposited SnO_2. Measuring the surface area of the deposited film, taking account of SnO_2 specific weight of the film, thickness was determined using the relation:

$$T = M_{SnO2}/A*\rho *10^4 \quad \text{---------- (2)}$$

where
A = Surface area of the film [cm^2]
M_{SnO2} = Quantity of the deposited tin oxide
ρ = Specific weight of SnO_2.

The calculated values of the film thickness are given in Table 2.

3. 2. X-ray diffraction analysis

The XRD patterns of as-deposited nanostructured SnO_2 thin films as function of deposition temperatures are shown in Fig. 1. The crystallite size, dislocation density and microstrain were estimated form the XRD pattern.

The crystallite size was estimated using Scherrer's formulla was given in Table 2.

$$D = 0{\cdot}9\lambda/\beta\cos\theta \quad \text{---------- (3)}$$

where, D = Average crystalline size
λ = X-ray wavelength (1·5418 Å)
β = FWHM of the peak
θ = Diffraction peak position.

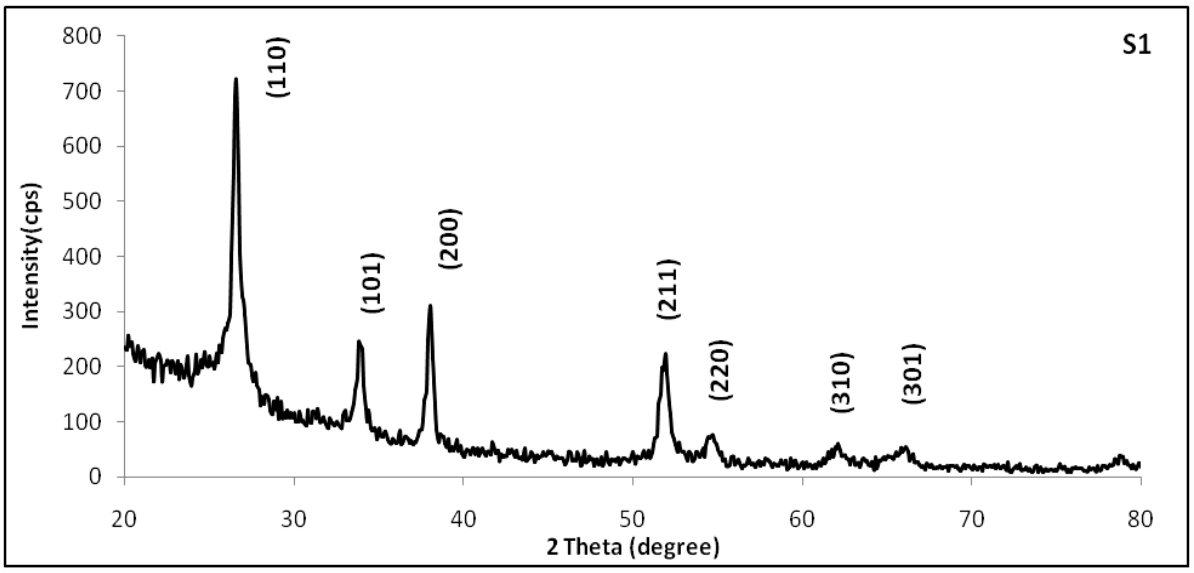

(a)

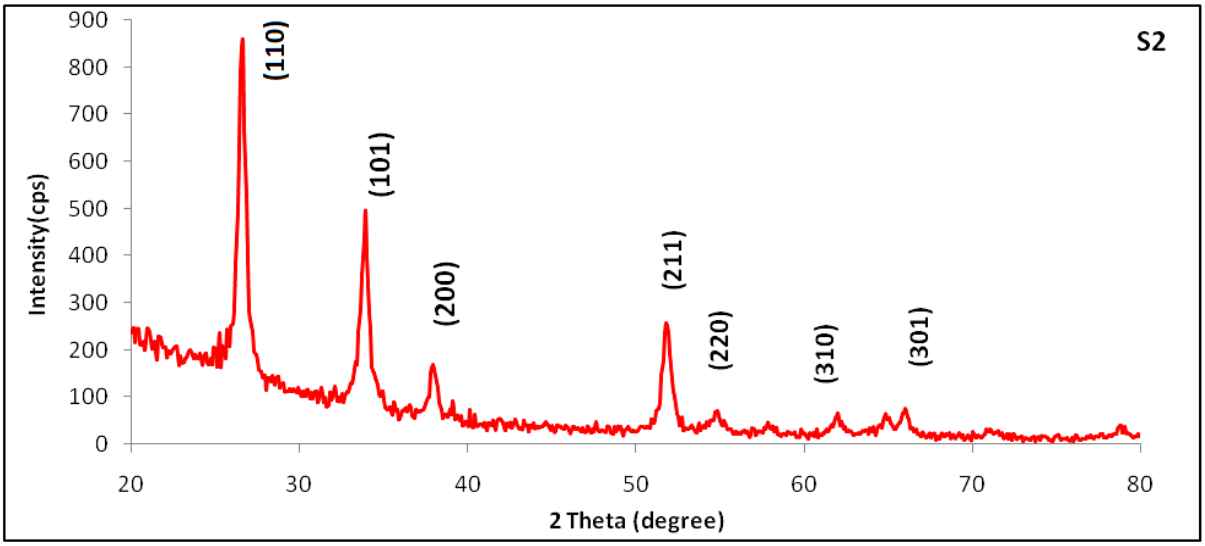

(b)

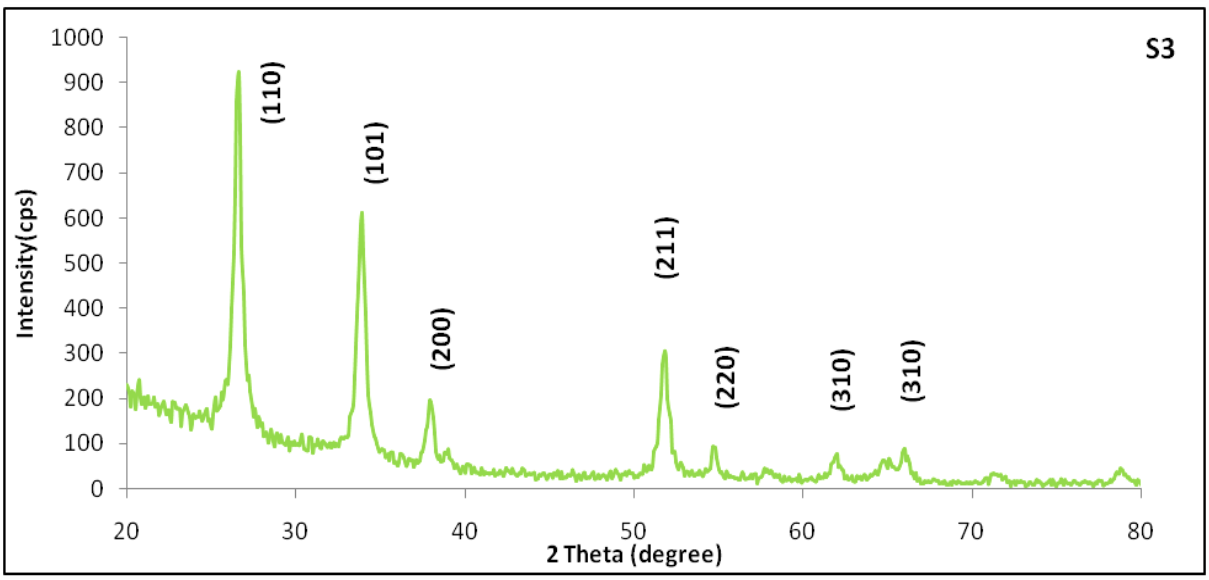

(c)

Fig. 1. X-ray diffractogram of nanostructured SnO_2 thin films samples: (a) S1, (b) S2, and (c) S3.

The observed peaks (110), (101), (200), (211), (220), (310) and (301) in the XRD pattern are matching well with the reported ASTM data of pure SnO_2 [15]. The intensity of the peaks increases with increasing deposition temperature. Especially, the intensity of the major peaks (110), (101), and (211) dominantly increased with increasing spray deposition temperature up to 400 °C.

Dislocation density values were calculated using the standard relations [16]:

$$\text{Dislocation density} \quad (\delta) = 1/D^2 \quad \text{----------(4)}$$

The dislocation density value was tabulated in Table 2.

3. 2. 1. Microstructural Details

Broadening of X-ray diffraction line profiles is mainly caused by non-ideal optics of the instrument, wavelength dispersion, and micro structural imperfections in the crystals. The micro structural line broadening can be subdivided into size broadening and strain broadening. Size broadening is due to the finite size of domains surrounded by stacking faults, by twins or other imperfections, which diffract incoherently with respect to one another. Strain broadening is caused by a varying displacement of the atoms with respect to their reference-lattice positions. The prepared SnO_2 thin films was nanocrystalline in nature, and hence large number of grains with various relative positions and orientation cause variations in the phase difference between the wave scattered by all grain and other .The total intensity scattered by all grains is the sum of individual intensities scattered by each grain. On the other hand, lattice strain broadening is caused by varying displacement results in peak shift of X-ray diffraction lines [17], whereas a non-uniform tensile and compression strain results in broadening of diffraction lines (microstrain). Thus grain size and microstrain effects are interconnected in the line broadening of peaks which make it difficult to separate.

According to the Williamson – Hall technique (Williamson and Hall 1953), it is assumed that both the crystalline size and microstrain broadened profiles are lorentzian [18,19]. Based on this assumption, a mathematical relation was established between the integral breadth (β), the volume of weighted average crystalline size (D) given by Eq. (5)

$$\beta \cos\theta/\lambda = 1/D + \varepsilon (\sin\theta/\lambda) \quad \text{--------} \quad (5)$$

where;
β = full width at half maxima of peak measured in radian
θ = diffraction angle
λ = wavelength of X-ray
D = grain size
ε = microstrain

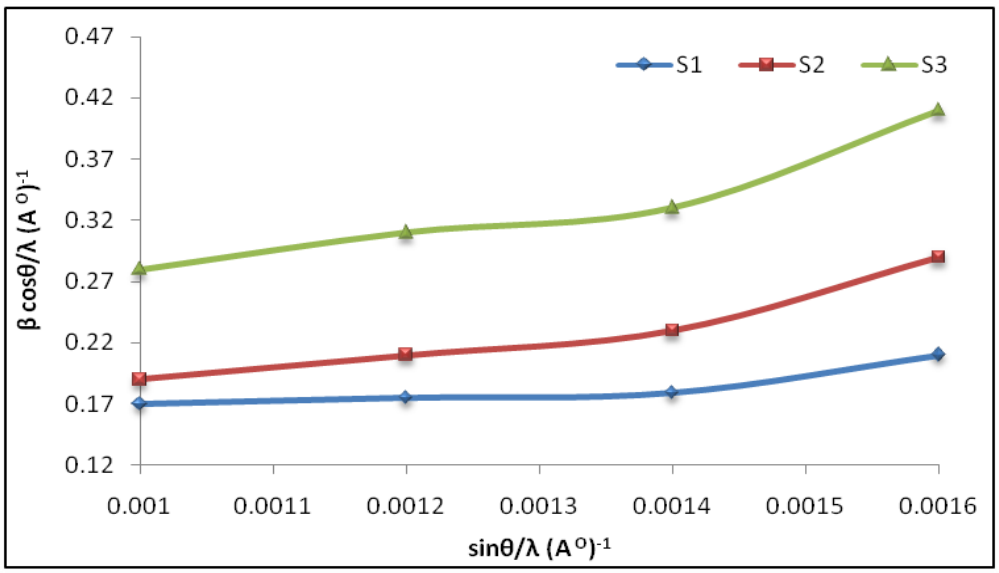

Fig. 2. Variation of β cosθ/λ with sinθ/λ.

The slope of the plot between β cosθ/λ and sinθ/λ gives microstrain and inverse of intercept of y-axis gives grain size Fig. 2 shows the Williamson- Hall plot of SnO_2 [6] thin films prepared from spray pyrolysis temperature. It shows that as there is increase in spray pyrolysis temperature, crystalline size increases from 23 nm to 36 nm as well as decrease in microstrain values from 2.6 x 10^{-3} to 0.96 x 10^{-3}.

Table 2. Measurement of spray pyrolysis temperature, film thickness, crystalline size, grain size, dislocation density and microstrain.

Sample	Spray deposition temp. (^oC)	Thickness (nm)	Crystalline size from XRD (nm)	Grain size from SEM (nm)	Dislocation density (10^{15})	Microstrain (arb. unit)
S1	300	289	23	26	4.3	2.6 x 10^{-3}
S2	350	210	29	32	3.4	1.9 x 10^{-3}
S3	400	180	36	39	2.7	0.96 x 10^{-3}

It is observed from Table 2 that as spray pyrolysis temperature increases, the thickness of the film was varied from 289 to 180 nm. It was found that as spray pyrolysis temperature increases, crystallite size, grain sizes are goes on increasing with decrease in dislocation density and microstrain.

3. 3. Surface Morphology

3. 3. 1. Scanning electron microscope

The microstructure of the prepared film was analyzed using a scanning electron microscope (SEM, JEOL. JED 6300).

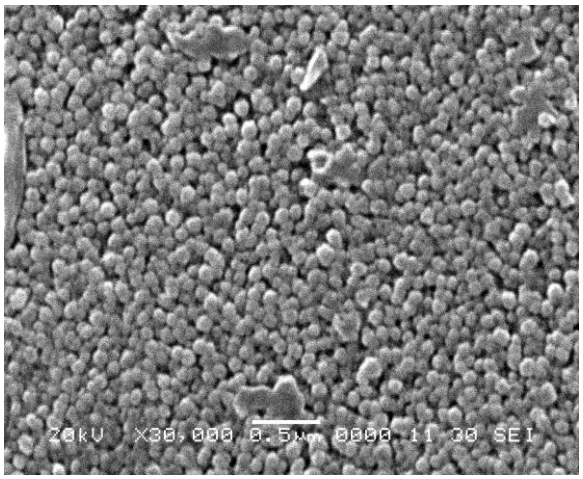

(a)

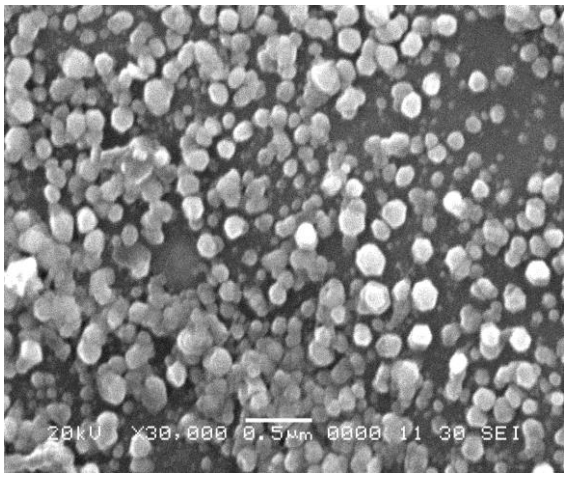

(b)

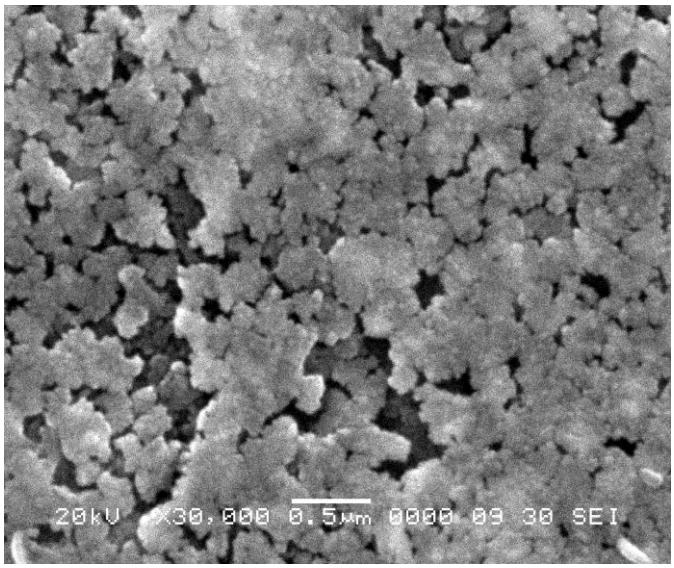

(c)

Fig. 3. SEM images of nanostructured SnO_2: (a) S1, (b) S2, and (c) S3.

Fig. 3 (a - c) shows the SEM images of nanostructured SnO_2 thin film samples S1, S2, and S3 respectively. From micrographs one can see that nanostructured SnO_2 is formed on the surface of the thin films. Fig. 3 (a) and (b) shows grains are spherical in shape. When spray depositon temperature was increased, increase in grain size of spherical shape was observed in Fig. 3 (b) and (c). From this behavior we point out that the grain size increased with increase in spray deposition temperature of thin films. In Fig. 3 (a) and (b) grains are uniformly distributed and Fig. 3 (c) show agglomeration of grains. Thus the grain size goes on increasing and smoothness goes on decreasing with the increase in spray deposition temperature. It may be due to collapse of larger grains into smaller with the increase in spray deposition temperature. The observed grain sizes were tabulated and presented in Table 2.

3. 4. Quantitative elemental analysis (EDAX)

Table 3. Quantative elemental analysis as prepared nanocrystalline SnO_2thin film.

Element	**Observed**					
	Sample S1 ($T_{pyro.}$ = 300 °C)		Sample S2 ($T_{pyro.}$ = 350 °C)		Sample S3 ($T_{pyro.}$ = 400 °C)	
	mass %	at %	mass %	at %	mass %	at %
Sn	75.77	29.58	75.50	27.67	78.31	26.41
O	24.23	70.42	24.50	72.33	21.69	73.59
SnO_2	100.00	100.00	100.00	100.00	100.00	100.00

The quantative elemental composition of the thin film sample was analyzed using an energy dispersive spectrometer. Stoichiometrically expected at % of Sn and O is: 33.30 and 66.70, respectively, observed at % of Sn and O were tabulated in Table 3.

There is little deviation from stoichiometry of the prepared film. Hence as prepared thin films were nonstoichiometry in nature.

4. MEASUREMENT OF ELECTRICAL PROPERTIES

4. 1. I–V characteristics

The sensor structures were prepared in dimension as: 1.5 cm × 1 cm. The contacts were made by silver paste on thin film surface. Figure 4 shows the I–V characteristics of samples S1, S2, and S3 observed to be nearly symmetrical in nature indicating ohmic contacts. The non-linear I–V characteristics may be due to semiconducting nature of the films.

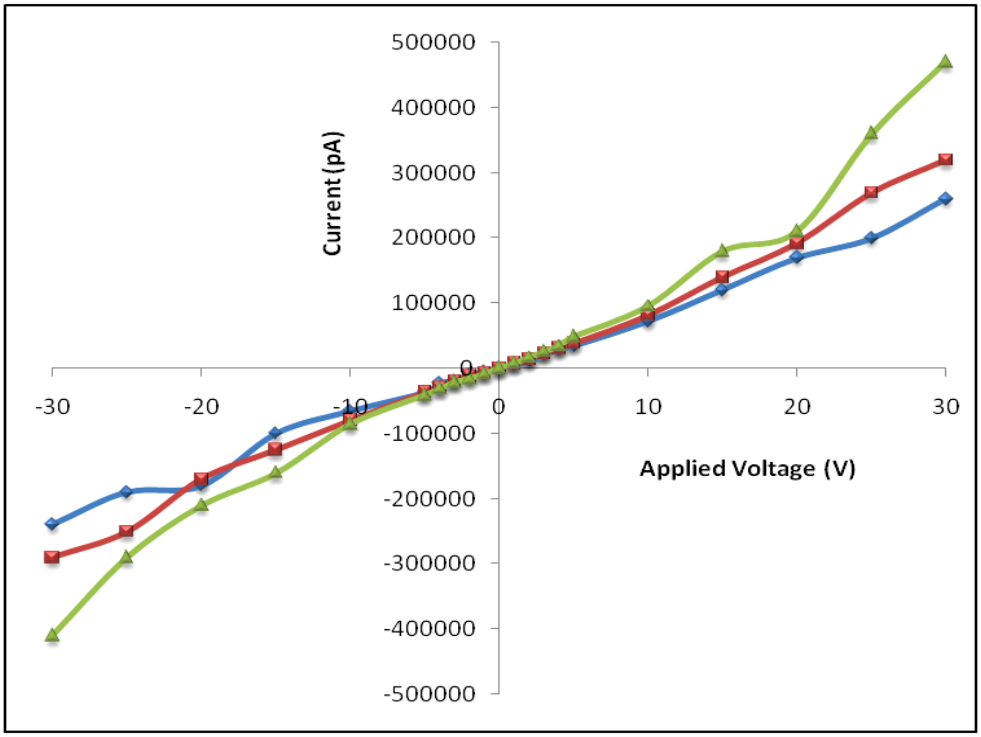

Fig. 4. I–V characteristics of nanostructured SnO_2 thin film sensors.

4. 2. Electrical conductivity

The electrical conductivity characterization was carried out in a static gas sensing unit with a temperature controller. A constant voltage was applied to the sample and the variation of current was measured. The variation of current with temperature was recorded during the cooling as well. Electrical conductivity was calculated from the dimensions of the samples. Figure 5 shows the log (σ) versus 1000/T curves of samples S1, S2 and S3 at different film thickness. A hysterisis behavior was observed in all samples. Two distinct regions in the conductivity curves was observed at a high temperature region from 200 °C to 400 °C.

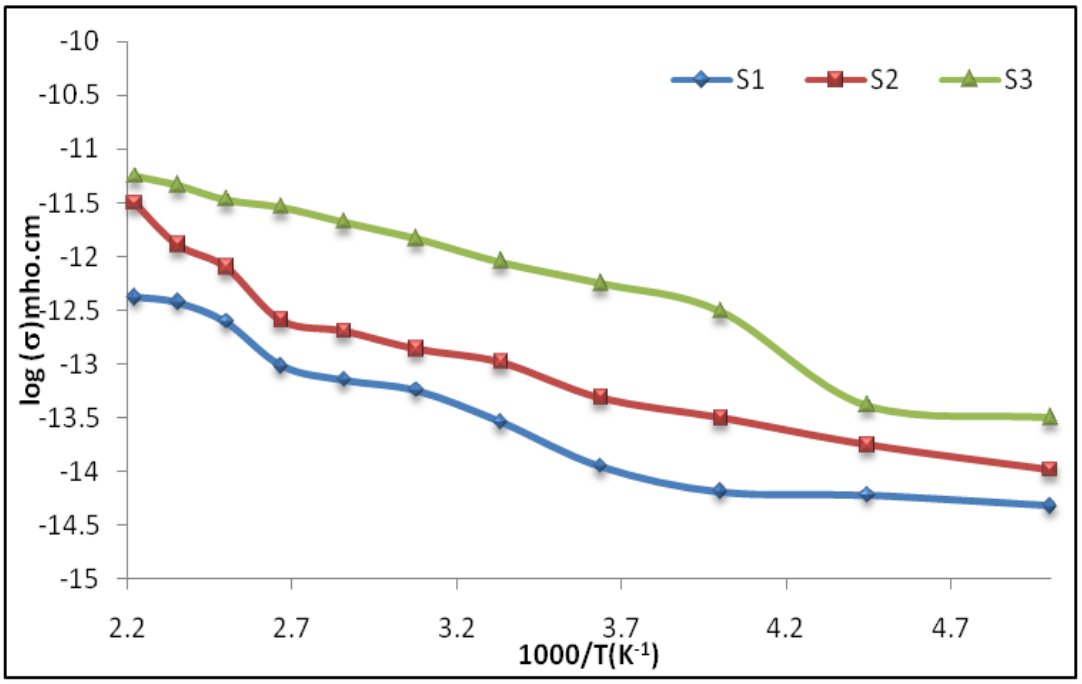

Fig. 5. Variation of log (σ) with operating temperature (°C).

In general, the electrical conductivity increases, as the film thickness increases, since the grain size is raised with the thickness. Consequently grain boundary scattering diminished by the reduction of the number of grain boundaries. The film conductivity increases linearly with increasing temperature indicating the semiconducting behavior of the SnO_2. Consequently, the activation energy *Ea* was calculated by applying the conductivity relation [36]:

$$\sigma = \sigma\, o \exp(-Ea/kT) \quad \text{---------- (6)}$$

where, σ is the conductivity,
σ *o* is a constant,
k is Boltzmann constant
and 'T' is the temperature.

The conductivity studies on films show that all the films exhibit two activation energies at different temperature regions. These activation energies vary with film thickness and are listed in Table 4. The results indicate the presence of two donor levels - one deep and one shallow near the bottom of the conduction band. Both of these levels depend on the film thickness. It can be seen that, in high temperature region (200 °C to 400 °C) activation energy values decreased in all samples.

For the metal oxide semiconductor thin films it is reported that [9,20], when thickness of the film decreases activation energy goes on increasing. It is clear from Table 4 that, as film thickness of the sample goes on decreasing; while the activation energy goes on increasing. The increase in activation energy with decreasing film thickness may be due to the change in structural parameters, improvement in crystallite and grain size [18].

Table 4. Measurement of activation energy and film thickness.

Sample no.	Thickness (nm)	Activation energy (ΔE)	
		200 °C	400 °C
S1	289	0.21 eV	0.29 eV
S2	210	0.39 eV	0.51 eV
S3	180	0.50 eV	0.62 eV

5. GAS SENSING PERFORMANCE OF THE SENSORS

5. 1. Measurement of gas response

Gas response (S) of the sensor is defined as the ratio of change in conductance to the conductance of the sensor on exposure of target (at same operating conditions).

$$S = G_g - G_a/G_a \quad \text{----------} \quad (7)$$

where;
G_a = the conductance of the sensor in air
G_g = the conductance on exposure of a target gas.

Figure 6 shows the variation in response with the operating temperature to 500 ppm of H_2 for S1, S2, and S3 samples. For all the samples the response increases with increase in operating temperature and reach maximum (S = 1200 for sample S2) at 350 °C.

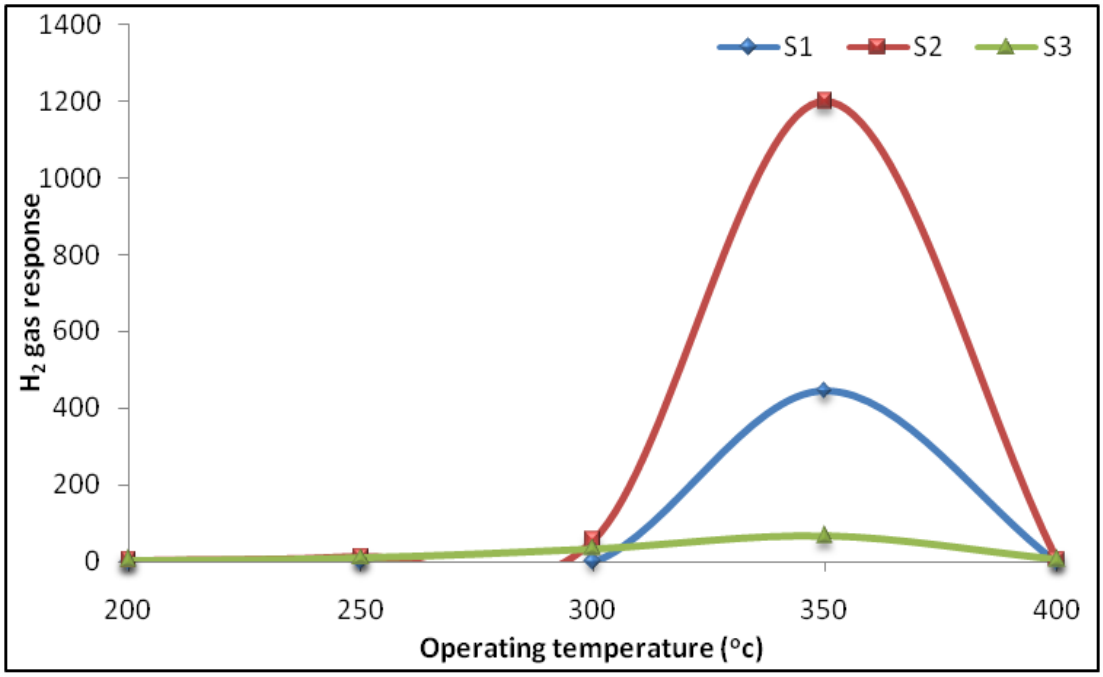

Fig. 6. Gas response of pure nanostructured SnO_2 thin films with operating temperature.

Response of sensors depends on two factors, namely: the speed of chemical reaction on the surface of the grains, and the speed of the diffusion of gas molecules to that surface. At low temperatures the sensor response is restricted by the speed of chemical reactions. At higher temperature the sensor response is restricted by the speed of the diffusion of gas molecules to that surface.

At some intermediate temperature the speed values of two processes become equal, and at that point the sensor response reaches its maximum. According to this mechanism for every gas there is a specific temperature at which the sensor response attains its peak value.

5. 2. Selectivity

Selectivity can be defined as the ability of a sensor to respond to a certain gas in the presence of different gases. Fig 7 shows the histogram for comparison of the H_2 response to various gases for sample S1, S2, S3 at the optimum operating temperature 350 °C. The table attached to histogram (Fig. 7) shows the gas response values, it is clear that the S2 film is highly selective to H_2 (500 ppm) against all other tested gases: LPG, CO_2, CO, NH_3, C_2H_5OH, Cl_2 NO_2, NO, SO_2 and H_2S.

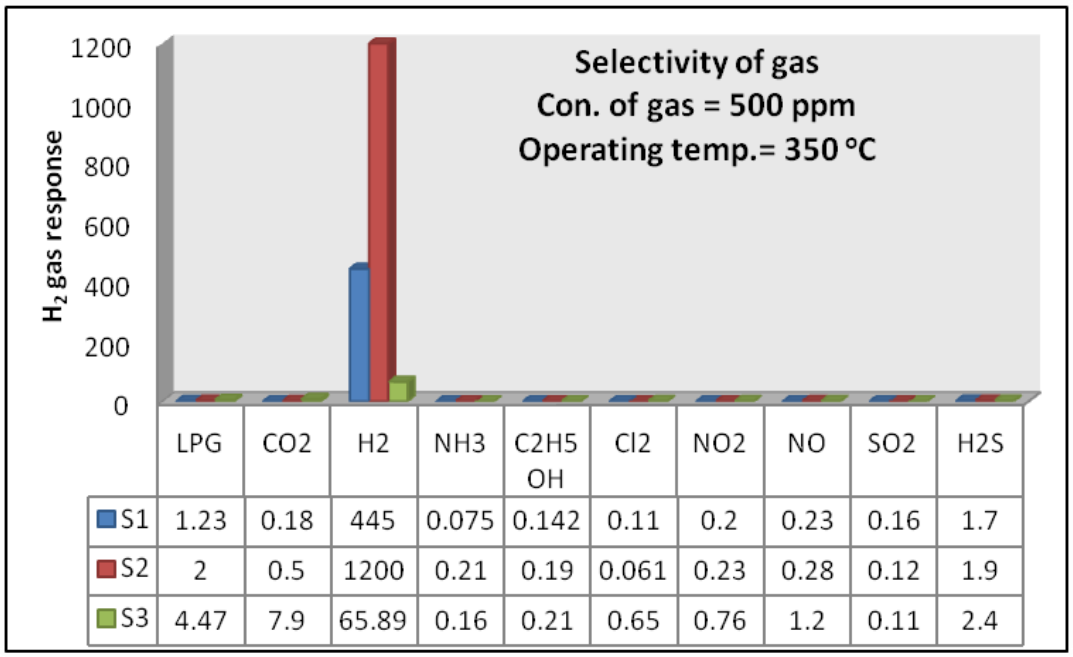

	LPG	CO2	H2	NH3	C2H5 OH	Cl2	NO2	NO	SO2	H2S
S1	1.23	0.18	445	0.075	0.142	0.11	0.2	0.23	0.16	1.7
S2	2	0.5	1200	0.21	0.19	0.061	0.23	0.28	0.12	1.9
S3	4.47	7.9	65.89	0.16	0.21	0.65	0.76	1.2	0.11	2.4

Fig. 7. Selectivity of nanostructured SnO_2 thin films for different gases.

5. 3. Response and recovery of the sensor

The time taken for the sensor to attain 90 % of the maximum decrease in resistance on exposure to the target gas is the response time. The time taken for the sensor to get back 90 % of original resistance is the recovery time. The response and recovery of the nanostructured SnO_2 thin film (S2) sensor on exposure of 500 ppm of H_2 at 350 °C are represented in Fig. 8. The response is quick (7 s) and recovery is fast (8 s). The high oxidizing ability of adsorbed oxygen species on the surface nanoparticles and high volatility of desorbed by-products explain the quick response to H_2 and fast recovery.

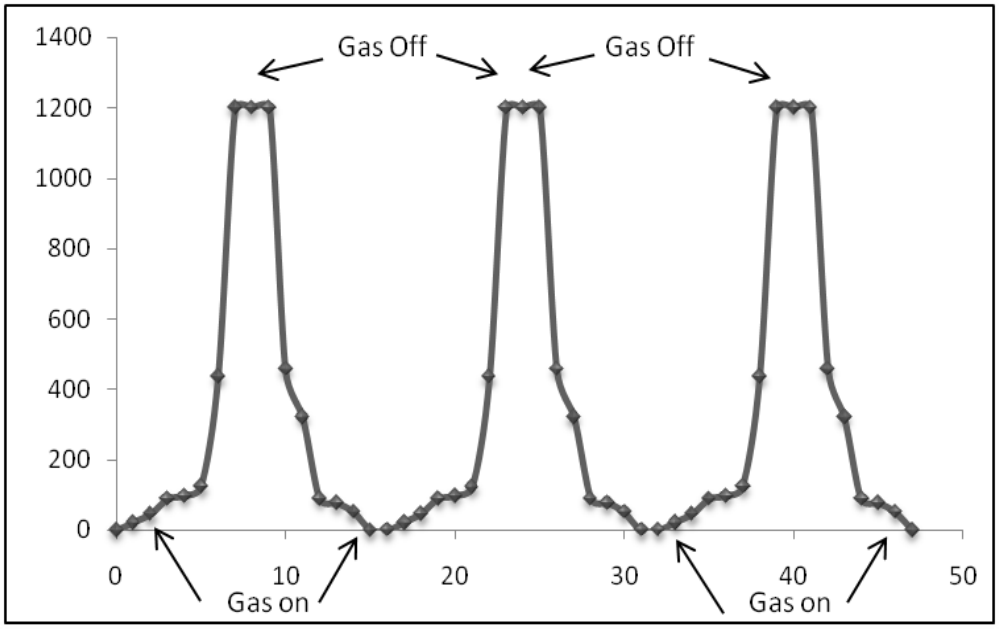

Fig. 8. Response and recovery of the sensor (Sample = S2).

The time taken for the sensor to attain 90 % of the maximum decrease in resistance on exposure to the target gas is the response time. The time taken for the sensor to get back 90 % of original resistance is the recovery time. The response and recovery of the nanostructured SnO_2 thin film (S2) sensor on exposure of 500 ppm of H_2 at 350 °C are represented in Fig. 8. The response is quick (7 s) and recovery is fast (8 s). The high oxidizing ability of adsorbed oxygen species on the surface nanoparticles and high volatility of desorbed by-products explain the quick response to H_2 and fast recovery.

6. DISCUSSION

Nano structured metal oxide semiconductors such as ZnO, SnO_2, TiO_2 and WO_3 [21-28] are widely used as gas sensors, as their resistivity changes in the presence of reactive gases [29,30]. Nanostructures are attractive as sensing elements owing to their large surface area to volume ratio allowing higher adsorption of gas molecules. Ionosorption of the analyte species over the surface of the metal sensing material is the fundamental phenomenon behind the sensing process with carbon, oxygen and water being the most important ionosorbed species [31]. The preferable operating temperature for semiconductor gas sensors ranges between 200 °C and 500 °C. At temperatures below 200 °C, oxygen is adsorbed in molecular form (neutral or charged).

When the temperature is increased, the adsorbed oxygen molecule dissociates into atomic oxygen (neutral, singly or doubly charged), and when the temperature is too high, oxygen atoms desorbs from the sensor. Exposure to reducing gases changes the density of ionosorbed oxygen that alters the sensor conductance. The conductance of n-type oxides increases in the presence of reducing gases and decreases in the presence of oxidizing gases, and the opposite behavior is observed for p-type metal oxides.

Gas sensors based on n-type semiconductors like SnO_2 and ZnO have been studied for the detection of inflammable or toxic gases such as H_2, CH_4, C_2H_5OH, CO or LPG [32-39].

Gas sensing mechanism is generally explained in terms of change in conductance due to the interaction of test gases with the semiconducting surface as shown in Fig. 9. The change of conductance is either by adsorption of atmospheric oxygen on the surface and/or by direct reaction of lattice oxygen or interstitial oxygen with the test gases. In case of former, the atmospheric oxygen adsorbs on the surface by extracting an electron from the conduction band, in the form of super oxides or peroxide, which are mainly responsible for the detection of the test gases.

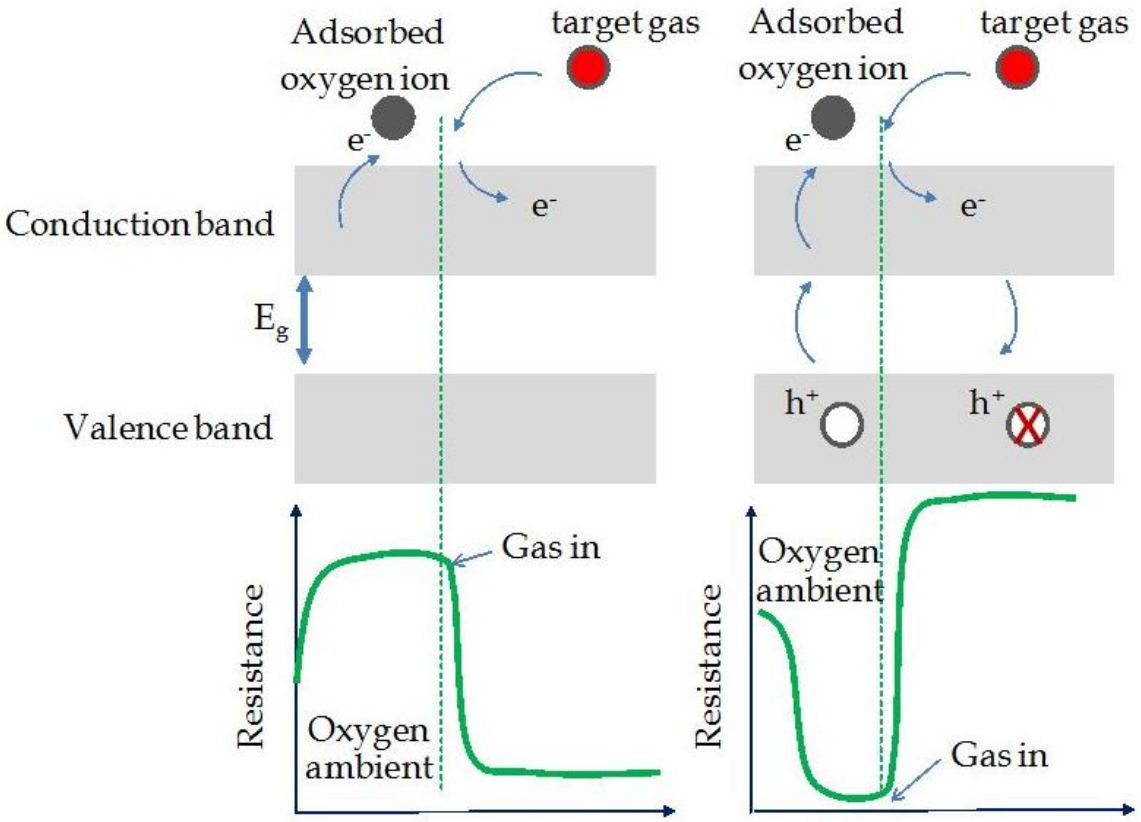

Fig. 9. Gas sensing mechanism.

The most important features of the present investigation are: high gas response, high selectivity to particular gas against other gases, fast response and quick recovery. The enhanced response could be attributed to nanocrystalline nature of the films [40]. It is known that when SnO_2 semiconductor thin film is exposed to air, physisorbed oxygen molecules pick up electrons from the conduction band of SnO_2 and change to O_2 - ads or O- ads species as indicated in equations (8) and (9),

$$O_{2\,(gas)} + e^- \rightarrow O^{2-}{}_{(ads)} \text{ ---------- (8)}$$

$$O^{2-}{}_{(ads)} + e^- \rightarrow 2O^-{}_{(ads)} \text{ ---------- (9)}$$

Before exposure of H_2, SnO_2 nanoparticles are depleted of electrons from the conduction band by oxygen species (O_2, O^- and O^{2-}) adsorbed on particle surface forming an electron depletion layer on particle surface which increases the sensor resistance.

Under H_2 exposure, a surface reaction reduces the coverage of oxygen, causing returning electrons to SnO_2 [6] by the following reactions:

$$2H_{2\ (gas)} + O^{2-} \rightarrow 2H_2O_{(vap.)} + e^- \quad \text{----------} \quad (10)$$

$$H_{2\ (gas)} + O_{(ads)} \rightarrow H_2O_{(vap.)} + e^- \quad \text{----------} \quad (11)$$

The extra electrons released in this process enhance the surface conductance of the thin film. The model proposed above, explains the gas sensing mechanism of the SnO_2 thin film sensor qualitatively. But it does not explain the increase in gas response with rise in operating temperature (Fig. 10). In this connection, the microstructure, particularly the size and distribution of surface porosity may also have a significant role. This is so because the surface SnO_2 thin film may provide suitable chemisorptions sites, and hence can influence the extent as well as the kinetics of the oxidation reaction (Eq. 8) between the sensor surface and the surrounding gas ambient.

Therefore, it is suggested that uniform granular distribution would cause high response has been observed in the present work.

7. CONCLUSIONS

Thin films of SnO_2 can be deposited on glass substrates by spray pyrolysis technique. The structural and microstructural properties confirm that the as-prepared SnO_2 thin films were nanostructured in nature. The EDAX of the films indicated that the SnO_2 thin films were nonstoichiometric. As deposition temperature increases, crystallite size, grain size also increases. Thickness of the films, dislocation density and microstrain decreases with increase in deposition temperature SnO_2 thin film sensor showed a high response (S2 = 1200) to H_2 gas in a wide concentration range at operating temperature 350 °C. The sensor showed good selectivity to H_2 gas against LPG, CO_2, CO, NH_3, C_2H_5OH, Cl_2, NO_2, NO, SO_2 and H_2S gases. The nanostructured SnO_2 thin film exhibits rapid response-recovery which is one of the main features of this sensor. The results obtained by spray pyrolysis technique (SPT) are promising for the preparation of sensitive and low cost hydrogen sensor operating at high temperatures.

Acknowledgements

The authors are thankful to the University Grants Commission, New Delhi for providing financial support. Thanks to Principal, G. D. M. Arts, K. R. N. Commerce and M.D. Science College, Jamner, for providing laboratory facilities for this work.

Reference

[1] C. Wang, X. F. Chu, M. M. Wu, *Sensors and Actuators B,* 120 (2007) 508.

[2] J. Kaur, R. Kumar, M. C. Bhatnagar, *Sensors and Actuators B* 126 (2007) 478.

[3] J. Isidorsson, C. G. Granquist, *Solar Cells* 44 (1996)375.

[4] K. L. Chopra, S. Major, D. K. Pandya, *Thin Solid Films* 102 (1983) 1.

[5] B. Stjerna, E. Olsson, C. G. Granquist, *Journal of Applied Physics* 76 (1994) 3797.

[6] L.A. Patil, M.D. Shinde, A. R. Bari, V. V. Deo, *Sensors and Actuators B* 143 (2009) 270.

[7] T. Okuno, T. Oshima, S. Dong Lee, S. Fujita, *Physica Status Solidi* 8 (2011) 540.

[8] H. S. Randhawa, M. D. Matthews, R. F. Bunshah, *Thin Solid Films* 83 (1981) 267.

[9] T. Mohanty, Y. Batra, A. Tripathi, D. Kanjilal, *Journal of Nanoscience and Nanotechnolology* 7 (2007) 2036.

[10] T. Gui, L.Hao, J. Wang, L. Yuan, W. Jai, X. Dong, *Chineses Optics Letters* 8 (2010) S10134

[11] J. Liu, S. Gong, J. Xia, L. Quan, H.Liu, D. Zhou, *Sensors and Actuators B* 138 (2009) 289.

[12] R. J. Deokate, S. V. Salunkhe, G. L. Agawane, B. S. Pawar, S. M. Pawar, K. Y. Rajpure, A. V. Moholkarb, J. H. Kimb, *Journal of Alloys and Compounds* 496 (2010) 357.

[13] R. H. Bari, R. S. Khadayate, S. B. Patil, A. R. Bari, G. H. Jain, L. A. Patil, B. B. Kale, *ISRN Nanotechnology*, ID 734325, (2012) 5.

[14] S. D. Sartale, C. D Lokhande, *Materials Chemistry and Physics* 72 (2001) 101.

[15] ASTM card no.05-0467.

[16] C. K. De, N. K. Mishra, *Indian Journal of Physics* 71 (1997) 530.

[17] Sciti D., Celotti, Pezzotti G., Guicciardi S., *Applied Physics A* 86 (2009) 243.

[18] A. Sarkar, P. Mukherjee, P. Barat, *Condensed Matter Materials Science arxiv.org, Cond-mat* 08 (2007) 10701645.

[19] G. K. Willamson, W. H. Hall, *Acta. Metal* 1 (1953) 22.

[20] K. C. Sharma, J. C. Garg, *Phyics. D: Applied Physics* 23 (1990) 1411.

[21] T. Ishihara, K.Kometani, M.Hashida, Y.Takita, *Journal of Electrochemical Society* 138 (1991) 173.

[22] Kashyout A. B., Soliman H. M. A., Shokry Hassan, Abousehly A. M., *Journal of Nanomaterial* (2010) 341841.

[23] I. C. Yao, P. Lin, T. Y. Tseng, *Advance Science Letter* 3 (2010) 548.

[24] J. Chen, J. Li , G .Xiao and X .Yang, *Journal of Alloys Compound*, 509, (2011)740.

[25] D. Barreca, D. Bekermann, E. Comini, A. Devi, R. A. Fischer, A. Gasparotto, C. MacCato, C. Sada, G. Sberveglieri, E .Tondello, *Cryst. Eng. Commun*. 12 (2010) 3419.

[26] W. Zeng, T. M. Liu, D. J. Liu, *Physica B* 405 (2010) 4235.

[27] M. R. Mohammadi, D. J. Fray, *Sensors and Actuators B* 150(6) (2010)31.

[28] J. Moon, J. A. Park, S. J. Lee, T. Zyung, I. D. Kim, *Sensors and Actuators B* 149 (2010) 301.

[29] S. J. Kim, I. S. Hwang, J. K. Choi, J. H. Lee, *Thin Solid Films* 519 (2010) 2020.

[30] T. D. Senguttuvan, V. Srivastava, J. S. Tawal, M. Mishra, S. Srivastava, K. Jain, *Sensors and Actuators B* 150 (2010) 384.

[31] N. Barsan, D. Koziej, U .Weimar, *Sensors and Actuators B* 121 (2007) 18.

[32] G. Korotcenkov, *Material Science and Engeeniring B* 139 (2007) 1.

[33] G. Korotcenkov, M. Ivanov, I. Blinov, J. R. Stetter, *Thin Solid Films* 515 (2007) 3987.

[34] O. Lupan, L. Chow, S. Shishiyanu, E. Monaico, T. Shishiyanu, V. Sontea, B. R. Cuenya, A. Naitabdi, S. Park, A. Schulte, *Material Research Bullien* 44 (2009) 63.

[35] M. C. Carotta, *Sensors Actuators B* 137 (2009) 164.

[36] S. M. Chou, L. G. Teoh, W. H. Lai, Y. H. Su, M. H. Hon, *Sensors* 6 (2006) 1420.

[37] E. Comini, G. Faglia, G. Sberveglieri, Z. L. Wang, *Appl. Phys. Lett*. 81 (2002) 1869.

[38] N. Koshizaki, T. Oyama, *Sensors and Actuators B* 66 (2000) 119.

[39] Y. I. Lee, K. J. Lee, D. H. Lee, Y. K. Jeong, Y. H. Choa, *Current Applied Physics* 9 (2009) S79.

[40] L. A. Patil, A. R. Bari, M. D. Shinde, Vinita Deo, M. P. Kaushik, *Sensors and Actuators B: Chemical* 161 (2012) 372.

(Received 06 June 2014; accepted 18 June 2014)